Mode of accretion in episodic radio galaxies and the dynamics of their outer relic lobes

Monthly Notices
of the
ROYAL ASTRONOMICAL SOCIETY

MNRAS **486,** 3975–3991 (2019)
Advance Access publication 2019 April 20

doi:10.1093/mnras/stz1089

Mode of accretion in episodic radio galaxies and the dynamics of their outer relic lobes

C. Konar,[1]★ M. J. Hardcastle,[2] J. H. Croston,[3] M. Jamrozy,[4] Ananda Hota[5] and Tapas K. Das[6,7]

[1]*Amity Institute of Applied Sciences, Amity University Uttar Pradesh, Sector-125, Noida-201303, U.P., India*
[2]*Centre for Astrophysics Research, School of Physics, Astronomy and Mathematics, University of Hertfordshire, College Lane, Hatfield AL10 9AB, UK*
[3]*School of Physical Sciences, The Open University, Walton Hall, Milton Keynes MK7 6AA, UK*
[4]*Obserwatorium Astronomiczne, Uniwersytet Jagielloński, ul. Orla 171, PL-30244 Kraków, Poland*
[5]*#eAstroLab , UM-DAE Centre for Excellence in Basic Sciences, Vidyanagari, Mumbai 400098, India*
[6]*Harish-Chandra Research Institute, Chhatnag Road, Jhunsi, Allahabad-211 010, India*
[7]*Physics and Applied Mathematics Unit, Indian Statistical Institute, Kolkata 700070, India*

Accepted 2019 January 25. Received 2019 January 22; in original form 2018 February 21

ABSTRACT

We present X-ray observations with the *X-ray Multi-Mirror Mission Newton* telescope of three double–double radio galaxies (DDRGs). We have detected the core, lobes, and environment of our sample DDRGs in X-rays. We examine the relationships between the radio and X-ray emission and attribute the X-ray emission from the lobes to the inverse Compton scattering of cosmic microwave background photons against the leptons of the radio lobes. The magnetic field strength of the lobes is close to the equipartition value. The X-ray spectrum of the cores of the DDRGs consists of an unabsorbed soft power-law component and no sign of hard power-law components. The soft unabsorbed component is likely to be related to the radio jets. In optical wavebands, there are no strong [O III] lines observed and the host galaxies are not detected in all four bands (namely 2.4, 4.6, 12, 22 μm) of the *Wide-Field Infrared Survey Explorer* survey. This shows that they are low-excitation radio galaxies. These DDRGs have poor group scale ambient media. We discuss the implications of this observation for models of the episodic activity in DDRGs.

Key words: galaxies: active – galaxies: individual: J0116–4722, J1158+2621, J1548–3216 – galaxies: jets – galaxies: nuclei – X-rays: galaxies.

1 INTRODUCTION

Radio galaxies are almost always hosted by massive elliptical galaxies with $M_{\rm gal} > 10^{10}\,{\rm M}_{\odot}$ or with black hole mass $M_{\bullet} > 10^{7}\,{\rm M}_{\odot}$ (since $M_{\bullet} \sim 10^{-3} M_{\rm gal}$ for ellipticals; see Fabian 2012). Only recently, a few cases have been found to be convincingly hosted by spiral or disc galaxies (Hota et al. 2011; Mulcahy et al. 2016 and references therein). A small fraction of radio galaxies, nearly 74 known so far, are episodic in nature (Kuźmicz et al. 2017). The majority of episodic radio galaxies (ERGs) are double–double radio galaxies (DDRGs; Schoenmakers et al. 2000a, 2000b) and two known cases are double–double radio quasars (DDRQs; Jamrozy, Saikia & Konar 2009; Nandi et al. 2014) and two spiral host episodic radio galaxies (*Speca*: Hota et al. 2011 and J2345−0449: Bagchi et al. 2014). Since ERGs occur in both elliptical and spiral host galaxies, and the jet originates from accretion on to supermassive black holes (SMBHs), the phenomenon of episodic jet formation has to have a close connection to the accretion physics rather than host galaxy or large-scale environment. To understand the reason behind the formation and cessation of jets, we first need to investigate the mode of accretion in DDRGs. We know that the bright central galaxies (BCGs) at the centre of galaxy clusters are very often radio loud and show signatures of episodic behaviour. These BCGs generally form FR I (Fanaroff & Riley 1974) radio galaxies and their episodic behaviour has been explained as due to a 'feedback loop' between the SMBHs and the ambient media via a Bondi-type hot accretion flow (McNamara & Nulsen 2007). However, it is important to study whether the episodic jet-forming activity in the FR II DDRGs can also be explained in terms of a 'feedback loop' between the SMBHs and the ambient media. Moreover, the cores of many of the DDRGs show variability even though they are radio galaxies and not quasars. Konar et al. (2013) have tentatively suggested that the core variability could be due to large variation of jet power, which then has to be associated with a large variation in the mass accretion rate.

★ E-mail: chiranjib.konar@gmail.com

Table 1. Observing log and source parameters. Exposure times are given after filtering for high particle background.

Object	Redshift	N_H 10^{22} cm^{-2}	Date	Exposure MOS1, MOS2, pn (s)
(1)	(2)	(3)	(4)	(5)
J0116−4722	0.1461	0.015	2009-11-28	57 650, 57 670, 42 460
J1158+2621	0.1121	0.017	2009-12-20	33 270, 33 670, 19 730
J1548−3216	0.1082	0.077	2010-02-03	22 480, 23 220, 11 230

A second key aspect of DDRGs is that their outer lobes are relic lobes, no longer connected to the jet, and hence are very diffuse in nature. In active FR II lobes the magnetic field is found to be generally within a factor of a few of equipartition (e.g. Croston et al., 2005; Ineson et al. 2017) but it is not clear how the disconnected lobes of DDRGs will evolve. Measuring the magnetic field in the relic lobes tells us about the evolution of the non-thermal plasma over a longer time. The objectives of this study are (i) to measure the magnetic field strength in the outer lobes of a sample of DDRGs, (ii) to determine the mode of accretion in these active galactic nuclei (AGNs), and (iii) to find which model(s) for explaining the episodic behaviour is/are consistent with the observations.

2 SAMPLE SELECTION

We carried out X-ray observations of a small sample of three DDRGs, namely J0116−4722, J1158+2621, and J1548−3216. We chose these DDRGs because they have (i) very diffuse outer lobes with back flow of relativistic plasma all the way to the core, (ii) inner jets propagating through the relic plasma of the outer lobes, and (iii) multifrequency radio data and spectral ageing analysis available. These criteria are required to study the dynamics of the outer lobes and inner jets. We have published the radio data in earlier papers (Konar et al. 2012, 2013; Konar & Hardcastle 2013). In this paper, the outer lobes of J0116−4722 are designated the N1 and S1 lobes for the northern and southern lobes, respectively. For J1158+2621, the outer lobes are designated the NW1 and SE1 lobes for the north-western and south-eastern lobes, respectively.

3 OBSERVATIONS AND DATA REDUCTION

3.1 Observations

We were allocated 57, 34, and 22 ks of *XMM* time for J0116−4722, J1158+2621, and J1548−3216, respectively. The observing log is given in Table 1.

3.2 Data reduction

We analysed the data with the *XMM–Newton* SAS version 12.5.0ac. The data analysis procedure is similar to what has been described in Croston et al. (2008). We ran EMCHAIN and EPCHAIN after we untarred the file. We generated good time interval (gti) files for MOS and pn data with RATE<0.35 and RATE<1.0 respectively, which were determined by looking at the light curve in the energy range 10–15 keV where X-rays are negligible. The filtering for the pn data was done with PATTERN ≤ 4 and ((FLAG & 0xfa000c)==0), and for the MOS data with PATTERN ≤ 12 and ((FLAG & 0x766a0600) = = 0) to exclude bad rows and columns.

3.3 Imaging

We have made a combined image out of the images from the MOS and pn cameras by adding them with appropriate weights so as to match the sensitivities of MOS cameras to that of the pn camera. Images were extracted within the energy range 0.4–7.0 keV using the task EVSELECT. The weights are determined by multiplying the background count ratios of the pn camera to MOS cameras. The exposure correction was then done in the combined image with the task EEXPMAP.

3.4 Spectral analysis

Spectral analysis was carried out for various regions, as described in Section 4, using the standard SAS spectral extraction tasks. Where small regions were analysed, and/or we wished to subtract the contribution of any diffuse environmental emission, we used a local background region, but for analysis of more extended regions we used double background subtraction, as described below.

3.4.1 Double background subtraction

The double background subtraction method accounts for the two backgrounds present in all *XMM* data – the astronomical background, which passes through the mirrors and so is vignetted, and the particle background, which is not – by subtracting the particle background from a local background region and then fitting a model to determine the level of the astronomical background. Correction for both the non-X-ray and X-ray background components is important to provide robust results for spectroscopy of large regions of diffuse emission.

The methods used here have previously been described by Croston et al. (2008). Briefly, we make use of 'filter-wheel closed' data sets that represent the expected particle background (Pontecouteau et al., private communication). These data sets were processed in the same way as the target source data sets, and were used by us for subtracting the particle background from our target data sets. The filter-wheel closed data sets have to be recast on to the target data sets to the physical coordinates, which is done using the task ATTCALC. Vignetting correction was done for the target data sets as well as the filter-wheel closed data sets using the SAS task EVIGWEIGHT. Since the exposure time of the filter-wheel closed data sets and the target source data sets are different, we determined the scaling factor in order to be able to subtract the particle background from the target source data sets in appropriate proportion. In order to estimate the scaling factor we measured the ratio of the count rate of target source data to filter-wheel closed data in the energy range 10–12 keV for the MOS data and 12–14 keV for the pn data. We took a large region (of order 600 arcsec in diameter) from the source and the background data sets in the above-mentioned energy ranges for MOS and pn cameras. The filter-

wheel closed data sets were scaled by the scaling factor before we carried out the background subtraction. If this scaling factor for a given camera is greater than approximately 1.7, then this double-background subtraction method will not work well for that camera. To extract the spectra in the double background subtraction method, we made use of the scaling factors (as described above) and the total exposure time. We then applied the corrections using a simple script that generates appropriate spectra and response files from the source and closed filter files using the SAS tasks EVSELECT, RMFGEN, and ARFGEN and scaled the background spectra appropriately.

All our data had relatively high particle background counts. For J1158+2621, the double background subtraction method worked (in the sense that the scaling factors were low enough to be usable) only for the pn data. Similarly, for J1548−3216 the methods work for MOS1 and MOS2 data and not for the pn data, and for the source J0116−4722 the double background subtraction method worked for none of the cameras. For J0116−4722, we instead used local background subtraction to constrain the spectra of the X-ray emission in the presence of the ambient medium (see Konar et al. 2009).

3.4.2 *Spectral fitting of the diffuse emission from the environment*

In all our spectral analysis we have grouped in bins of ≥20 counts in order for χ^2 statistics to be valid; spectra are then fitted in the standard manner in XSPEC.

For each source the local background spectrum, after correction for particle background by subtraction of the scaled closed-filter spectrum, was fitted with a composite model consisting of two *apec* (thermal bremsstrahlung) components and a power law (in XSPEC notation apec+apec+wabs(pow)). The two apec components are Galactic thermal emission and the emission from the local superbubble in our Galaxy. The power-law component is the cosmic X-ray background (CXB) radiation. An instrumental aluminium line appears in the energy range 1.4–1.8 keV. Whenever this line has appeared prominently in the spectrum, we have excluded that portion of the spectra before fitting our composite model. Two apec models have been fitted with solar abundance and for the power law the photon index was fixed to 1.41, though the normalization was a free parameter. The temperatures and normalizations of the two apec models were used as free parameters. For the power-law model we have used the Galactic neutral hydrogen column density from the Dickey & Lockman survey (Dickey & Lockman 1990). For the source (J0116−4722) for which we could not do the double background subtraction, we attempted to model the spectrum of diffuse X-ray emission using local background subtraction (see Croston et al. 2004; Konar et al. 2009). However, the temperature is poorly constrained and not at all reliable.

4 OBSERVATIONAL RESULTS

4.1 J0116−4722

We have previously published the Giant Metrewave Radio Telescope (GMRT) images of this source (Konar et al. 2013). Detailed spectral ageing analysis was not possible because of the limitations of the radio observations. It is clear from the radio images that this source has very diffuse lobe emission, which is ideal for the detection of inverse-Compton-scattered cosmic microwave background (CMB) photons in X-rays (hereafter, IC X-rays). We have tried to detect both thermal X-ray emission from the ambient medium and the IC X-rays from the lobes of this source. Because of the low count rate we could not constrain the spectrum, and hence the temperature, of the environment. It is likely from the low count rate of the environment that it is very poor.

4.1.1 *Core*

The X-ray image shows a point-like object at the radio core position. We put a circle as a source extraction region around the core position, and put an annulus around that circle as a background subtraction region (see the top left-hand panel of Fig. 1). The X-ray spectrum was extracted from the region of the radio core. Initially the spectral fitting was done between 0.3 and 8.0 keV. Plots of the spectrum and the best-fitting model are shown in the middle panel of Fig. 1. A single power-law fit with a photon index of 1.84 gives $\chi^2_{\rm red} = 3.08$ (the best-fitting parameters are not shown in the table for the single power-law fit). A single data point at around 6.0 keV does not fit to the single power law at all (see middle left-hand panel of Fig. 1). We therefore also fitted a double power-law model with intrinsic absorption (see the middle right-hand panel of Fig. 1). This fit yields an improved value of $\chi^2_{\rm red} = 1.66$; however, the column density of the torus is poorly constrained (see Model III in Table 2). Danziger & Goss (1983) mentioned the detection of [O III] emission (no spectra are available), which would be consistent with this being a radiatively efficient, obscured system (compare its properties with those of narrow-line radio galaxies discussed by Hardcastle, Evans & Croston 2009). However, our data do not allow us to constrain the torus column density properly. The non-detection of the source in the *Wide-Field Infrared Survey Explorer* (*WISE*) survey in band 4 (i.e. at 22 μm) suggests that the luminosity of any obscured nucleus is low or the column density of dust is lower than would normally be expected from a torus. Further X-ray observations and/or optical spectroscopic observations are required to accurately model this AGN system and its emission.

Since we cannot constrain the double power-law fit to the core X-ray spectra and there is a possibility of the presence of very little hard power law, we next tried to fit the data with a single power law between 0.3 and 5.5 keV range (see upper right-hand panel of Fig. 1 for the plot). We chose 0.3–5.5 keV as there is no prima facie evidence of a hard power law within this band. This fit is good with a photon index of 2.08 and $\chi^2_{\rm red} = 1.77$ (Model I of Table 2). We consider this model (i.e. Model I) to be the most acceptable model. We also tried to fit an *apec* model (fitted plot is not shown; for best-fitting parameters see Model II of Table 2) with the spectrum extracted from the position of the core and verified that the emission is not thermal, as the apec model (Model II of Table 2) fit is very poor with a value of $\chi^2_{\rm red} = 3.48$.

4.1.2 *Lobes*

We next examined the spectra of the lobes. Section 4.4 describes the details of the source extraction regions and background subtraction regions for the lobes . While extracting the spectra of the lobes, all the point sources within the lobes and the chip gaps were masked out. Since the background subtraction region is very far from the source, we would expect that the spectra of any given lobe consists of a thermal spectrum (i.e. an *apec* model) from the ambient medium and a power law for the IC X-rays from the lobes. However, we found that the fitting of a composite model consisting of an apec + a power law to the extracted spectra from either of

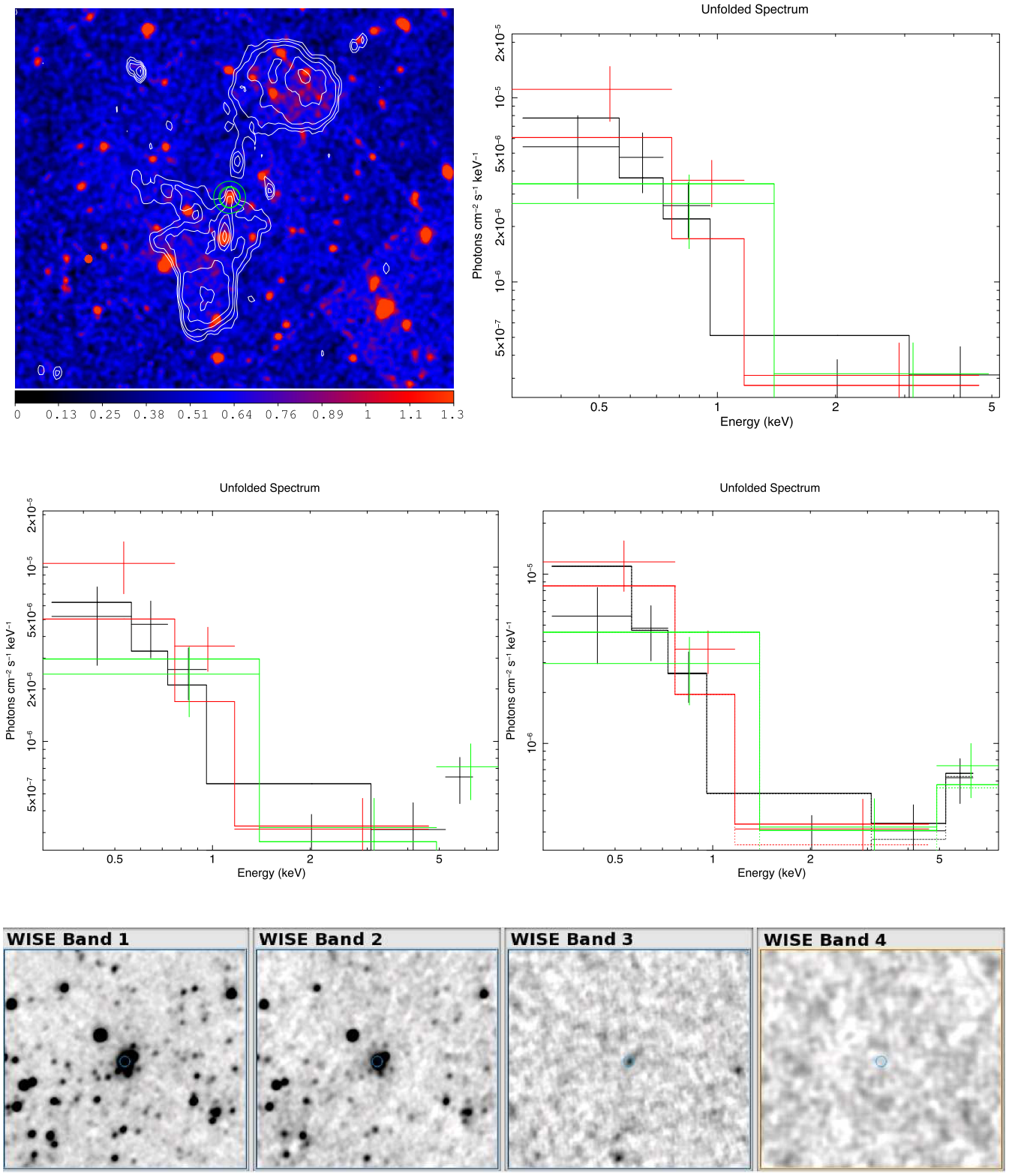

Figure 1. X-ray, radio, and mid-infrared properties of J0116−4722. Upper left-hand panel: an overlay of X-ray (colour) and radio (contour) images with the regions selected for the spectral extraction (contour details are given in Fig. 4). Upper right-hand panel: the X-ray spectrum of the core fitted with a single power law from 0.3 to 5.5 keV range. Middle left-hand panel: the X-ray spectrum of of the core fitted with a single power law from 0.3 to 8.0 keV. Middle right-hand panel: the X-ray spectrum of the core fitted with a double power law from 0.3 to 8.0 keV. Lower panel: *Wide-Field Infrared Survey Explorer* (*WISE*) images in four bands. The source is not detected in *WISE* band 4.

Table 2. Fits to and fitting statistics of the spectrum of the core of J0116−4722 ($N_{\rm H} = 1.5 \times 10^{20}$ cm^{-2}, $z = 0.146101$).

Model	Parameter	Model I	Model II	Model III
component		wabs(pow)	wabs(apec)	wabs(pow+zwabs(pow))
(1)	(2)	(3)	(4)	(5)
Core:				
Soft power law[a]	Γ	$2.08^{+0.53}_{-0.50}$		$2.37^{+0.57}_{-0.57}$
	1 keV flux density (nJy)	$1.05^{+0.24}_{-0.24}$ (preferred model)		$1.17^{+0.31}_{-0.24}$
Soft apec	kT (keV)		1.65 ± 0.33	
	Abundance		$0.3Z_{\odot}$ (frozen)	
	Unabsorbed flux (erg s^{-1} cm^{-2})		$(5.30 \pm 1.75) \times 10^{-15}$	
Hard power law	Nuclear $N_{\rm H}$ (cm^{-2})			$\left(58.97^{+127}_{-28.67}\right) \times 10^{22}$
	Γ			1.50 (frozen)
	Unabsorbed 1 keV flux (nJy)			$15.76^{+11.26}_{-20.78}$
$\chi^2_{\rm red}$		1.77	3.48	1.66
Environs:				
apec[b]	kT (keV)		11.28 ± 10.68	
	Abundance		$0.3Z_{\odot}$ (frozen)	
	Unabsorbed flux (erg s^{-1} cm^{-2})		$(5.90 \pm 1.90) \times 10^{-13}$	
$\chi^2_{\rm red}$			2.99	

Note. The apec spectrum has been integrated from 0.3 keV to 7 keV to find the flux.
[a]The only point between 5.5 and 8.0 keV was flagged, as it does not help to yield a better fit to any of the other plausible models listed in this table.
[b]The spectrum of the environment is not a good fit. The data are very bad.

the lobes is not good in the sense that they have absurd best-fitting values of the parameters with large errors (see Table 3), though we obtain reasonable $\chi^2_{\rm red}$ values. In fitting the composite model to the observed spectra of lobes, we found the ambient medium best-fitting temperature of 64 ± 519 keV for the N1 lobe and $0.05^{+0.04}_{-0.02}$ keV for the S1 lobe (see Table 3). These temperatures do not match with the temperature (11.28 ± 10.68 keV; see Table 2) constrained by fitting the apec model to the X-ray spectrum of the ambient medium. So, the ambient medium temperature is not at all reliable for J0116−4722. Moreover, we know from the data that the thermal X-ray from the ambient medium is very low as the number of counts is too low to be fitted. The flux for the apec component in the composite model fitting for the S1 lobe has a large error. The apec component seems to be negligible compared to the IC X-rays from the outer lobes. Visual inspection of the outer lobe spectra also shows that a single power-law fit to the outer lobe spectra looks reasonable. Therefore, we are justified in fitting only a single power-law fit to the outer lobe spectra of J0116−4722.

The single power-law fits to the outer lobe spectra yield photon indices of $1.77^{+0.12}_{-0.11}$ for the N1 lobe and $2.00^{+0.14}_{-0.13}$ for the S1 lobe (see Table 3). For the N1 lobe the photon index indicates an injection spectral index of $0.77^{+0.12}_{-0.11}$, which is consistent with the radio injection spectral index ($0.618^{+0.072}_{-0.065}$; Konar et al, 2013) of the non-thermal electrons constrained from the radio spectrum. However, the injection spectral index as implied by the S1 lobe photon index is $1.00^{+0.14}_{-0.13}$, which is slightly higher than the radio injection spectral index of $0.618^{+0.072}_{-0.065}$. There could be two reasons for such a discrepancy. (i) The injection spectral index of $0.618^{+0.072}_{-0.065}$ was measured from the total spectrum of the two lobes of J0116−4722, since we did not have radio flux density measurements for individual lobes at very low frequencies. Therefore, the discrepancy between the injection spectral index of the S1 lobe as constrained from the radio spectrum and the IC X-ray spectrum might be reconciled if we were to constrain the spectra of the two radio lobes separately down to very low frequencies. Our present observations do not permit us to make such measurements. (ii) There might be some contamination from the thermal X-ray emission from the ambient medium in the X-ray spectrum of the S1 lobe. We need better X-ray and radio observations to resolve this discrepancy.

4.2 J1158+2621

A detailed spectral ageing analysis of this object has been published by Konar et al. (2013).

4.2.1 Core

We have constrained the X-ray spectrum from the core region of this source by the same method as in the case of J0116−4722 by putting a circular region around the core as a source extraction region and an annular background region around the source extraction region for the background subtraction (for the details of the source extraction and background subtraction regions, see Section 4.4). We admit that there are little tight circles for the core spectral extraction and background subtraction. It is because if we increase the circle, then it will pick up the emission from the environment. As the core is

Table 3. Fits to and fitting statistics of the spectra of the lobes of J0116−4722 ($N_{\rm H} = 1.5 \times 10^{20}$ cm^{-2}, $z = 0.146101$).

Source component (1)	Model (2)	Parameter (3)	Best-fitting values (4)
N1 lobe	Power law	Γ	$1.77^{+0.12}_{-0.11}$
	(preferred model)	1 keV flux density (nJy)	$19.36^{+1.10}_{-1.10}$
		$\chi^2_{\rm red}$	1.42
	apec	kT (keV)	$5.42^{+2.07}_{-1.27}$
		Unabsorbed flux (erg s^{-1} cm^{-2})	$\left(1.61^{+0.09}_{-0.09}\right) \times 10^{-13}$
		$\chi^2_{\rm red}$	1.62
	apec + power law	Γ	$2.76^{+0.64}_{-0.52}$
		1 keV flux density (nJy)	$6.90^{+4.11}_{-2.88}$
		kT (keV)	64.00 ± 519
		Unabsorbed flux (erg s^{-1} cm^{-2})	$\left(1.34^{+0.28}_{-0.42}\right) \times 10^{-13}$
		χ^2_{red}	1.37
S1 lobe	Power law	Γ	$2.00^{+0.14}_{-0.13}$
	(preferred model)	1 keV flux density (nJy)	$18.17^{+1.10}_{-1.10}$
		$\chi^2_{\rm red}$	1.26
	apec	kT (keV)	$4.13^{+1.18}_{-0.84}$
		Unabsorbed flux (erg s^{-1} cm^{-2})	$\left(1.41^{+0.08}_{-0.08}\right) \times 10^{-13}$
		$\chi^2_{\rm red}$	1.66
	apec + power law	Γ	$1.81^{+0.17}_{-0.15}$
		1 keV flux density (nJy)	$17.41^{+1.16}_{-1.17}$
		kT (keV)	$0.05^{+0.04}_{-0.02}$
		Unabsorbed flux (erg s^{-1} cm^{-2})	$\left(1.70^{+55.5}_{-1.70}\right) \times 10^{-14}$
		$\chi^2_{\rm red}$	1.21

Note. The observed part (0.3–7.0 keV) of the spectrum has been integrated to find the flux of the apec model.

weak, it matters. So, we have to do the core spectral extraction with somewhat tight circles. What is important in our paper is to see the nature of the spectrum (single power law or double power law). We have done spectral extraction with various bigger circles around the core and we have presented the best one. The core spectrum is shown in the middle left-hand panel of Fig. 2. The core X-ray spectrum is a good fit to a single power law with a photon index of $\Gamma = 0.89$, which is very flat. The double power law and the apec model fits are not good, as the best-fitting parameters have large errors (see Table 4). So, we accept the single power law as the best model for the core X-ray spectrum. The core does not show the absorbed hard power law. The absence of an absorbed hard power law in the *XMM* band and [O III] line in the optical spectrum from SDSS (middle right-hand panel of Fig. 2), and the non-detection of this source in band 3 (12 μm) and band 4 (22 μm) of the *WISE* survey (bottom panel of Fig. 2) suggest that this AGN does not have any appreciable radiative output. Therefore, it is likely to possess no standard accretion disc (Shakura–Sunyaev disc; Shakura & Sunyaev 1973) around the SMBH in the central engine, and to be a low-excitation radio galaxy (LERG; Hardcastle et al. 2004).

4.2.2 *Environment*

For this source, we have been able to use the double background subtraction method (as described in Section 3.4.1) to constrain the spectrum of the thermal ambient medium. The best-fitting parameters are tabulated in Table 5. We have considered a large circular area around the core of J1158+2621 for the double background subtraction method to constrain the spectrum of the ambient medium. We masked out the core, radio lobes, and the point sources within the large circle (see the top left-hand panel of Fig. 2). We have been able to use only the pn data for this method as has been described in Section 3.4.1. The data from MOS cameras have large systematics and did not yield good results. The best-fitting temperature of the ambient medium is $0.81^{+0.08}_{-0.08}$ keV (see Table 5), which suggests a poor group scale environment (see e.g. fig. 13 of Osmond & Ponman 2004).

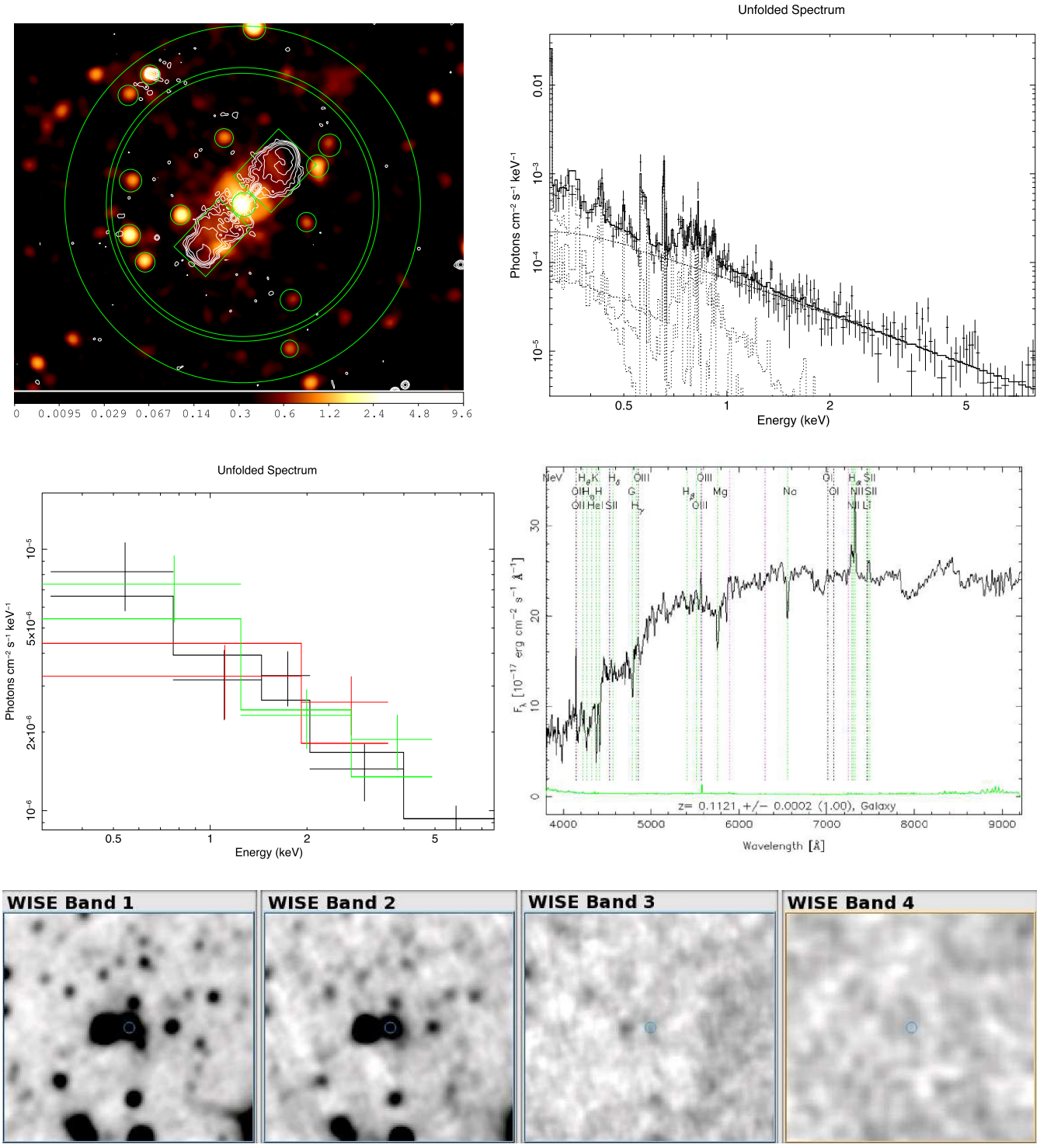

Figure 2. X-ray, radio, optical, and mid-IR properties of J1158+2621. Upper left-hand panel: the spectral extraction region for the environment using the double background subtraction method. GMRT *L*-band radio contours are overlaid on the X-ray (colour). The first radio contour is 0.5 mJy beam^{-1} with the other contours increasing by factors of 2. Upper right-hand panel: the best-fitting spectra of the environment and the three backgrounds (Galactic thermal emission, the emission from the local superbubble in our Galaxy, and the power-law cosmic X-ray background radiation). Middle left-hand panel: X-ray spectrum of the core of J1158+2621 in the 0.3–7.0 kev *XMM* band. The core spectrum is fitted with a single power law. Middle right-hand panel: SDSS optical spectrum from the core of the same DDRG. Lower panel: *WISE* images in four bands of the DDRG J1158+2621.

Table 4. Fitting statistics of the spectrum of the core of J1158+2621 ($N_{\rm H} = 0.017 \times 10^{22}$ cm^{-2}, $z = 0.112$).

Model component (1)	Parameter (2)	Model I wabs(pow) (3)	Model II wabs(apec) (4)	Model III wabs(pow+zwabs(pow)) (5)
Soft power law	Γ	$0.89^{+0.22}_{-0.22}$		1.92 ± 1.51
	1 keV flux density (nJy)	$2.87^{+0.59}_{-0.59}$ (preferred model)		2.20 ± 3.56
Soft apec	kT (keV)		64 ± 226	
	Unabsorbed flux (erg s^{-1} cm^{-2})		$(4.23 \pm 4.97) \times 10^{-14}$	
Hard power law	Nuclear $N_{\rm H}$ (cm^{-2})			$1.89 \pm 4.00 \times 10^{22}$
	Γ			1.34 ± 0.99
	Unabsorbed 1 keV flux (nJy)			4.98 ± 13.12
$\chi^2_{\rm red}$		0.90	1.77	1.15

Note. The apec spectrum has been integrated from 0.3 to 7 keV to find the flux.

Table 5. Fitting statistics of the background spectra of the environment of J1158+2621. Only data from the pn camera have been used. Because of the higher systematics, data from the MOS1 and MOS2 cameras could not yield any reasonable fit.

Model component (1)	Model parameter (2)	Best-fitting value (3)
Background spectrum-1	kT (keV)	$0.24^{+0.05}_{-0.03}$
	Abundance ($Z_\odot$)	1 (frozen)
	Redshift	0 (frozen)
	Norm (cgs)	$\left(2.13^{+0.43}_{-0.43}\right) \times 10^{-5}$
Background spectrum-2	kT (keV)	$0.041^{+0.002}_{-0.002}$
	Abundance ($Z_\odot$)	1 (frozen)
	Redshift	0 (frozen)
	Norm (cgs)	$\left(8.98^{+1.90}_{-1.97}\right) \times 10^{-3}$
Background spectrum-3	$N_{\rm H}$ (cm^{-2})	0.017×10^{22} (frozen)
	Photon index	1.41 (frozen)
	Norm ($N_{\rm 1keVph}$ s^{-1} cm^{-1})	$\left(6.16^{0.43}_{0.46}\right) \times 10^{-5}$
Thermal ambient medium	$N_{\rm H}$ (cm^{-2})	0.017×10^{22} (frozen)
	kT (keV)	$0.81^{+0.08}_{-0.08}$
	Abundance ($Z_\odot$)	0.3 (frozen)
	Redshift	0.112 (frozen)
	Norm (cgs)	$\left(7.33^{+1.01}_{-1.01}\right) \times 10^{-5}$

Note. The observed part (0.3–7.0 keV) of the spectrum has been integrated to find the flux of the apec model.

4.2.3 Lobes

We have not used the double background subtraction method for constraining the lobe-related X-rays, but instead used a single local background. (Section 4.4 describes the lobe extraction, background subtraction, and the chip gap regions). We set lobe extraction regions of the same size on both the lobes. We have assumed that the ambient medium is roughly (not exactly) spherically symmetric around the core. So we choose a background region of exactly the same size as the lobes and at a similar distance from the core so that the thermal emission from the line of sight (LoS) of the lobes is subtracted by a similar amount from the background region. However, some residual thermal emission might be there in the extracted lobe spectra as the thermal ambient medium may not be exactly spherically symmetric. So, the lobe-related X-rays (even after background subtraction) can be in principle a mixture of (i) IC X-ray and (ii) thermal X-ray (residual thermal X-rays along with possible X-rays generated by the shock-heated thermal gas due to fast expansion of the lobes). We fitted a power law to the SE1 lobe of J1158+2621 and had reasonably good best-fitting values for the parameters of this model with a value of $\chi^2_{\rm red} = 1.24$ (see Table 6). Best-fitting values of the photon index of $\Gamma = 1.95^{+0.35}_{-0.32}$ and 1 keV flux density of $3.46^{+0.81}_{-0.81}$ nJy have been obtained for the single power-law fit to the X-ray spectrum of the SE1 lobe. The photon index of $\Gamma = 1.95^{+0.35}_{-0.32}$ is very close to the value predicted from the injection spectral index $0.788^{+0.38}_{-0.40}$ constrained by fitting the spectral ageing model to the radio spectrum of the outer lobes of this DDRG. So the lobe-related X-rays are consistent

Table 6. Fitting statistics of the spectrum of the lobes of J1158+2621 ($N_{\rm H} = 0.017 \times 10^{22}\,{\rm cm}^{-2}$, $z = 0.112$).

Source component (1)	Model (2)	Parameter (3)	Best-fitting values (4)
SE1 lobe	Power law	Γ	$1.95^{+0.35}_{-0.32}$
	(preferred model)	1 keV flux density (nJy)	$3.46^{+0.81}_{-0.81}$
		$\chi^2_{\rm red}$	1.24
	apec	kT (keV)	$1.15^{+0.34}_{-0.22}$
		Unabsorbed flux (erg s^{-1} cm^{-2})	$\left(1.88^{+0.28}_{-0.24}\right) \times 10^{-14}$
		$\chi^2_{\rm red}$	0.51
	apec + power law	Γ	1.788 (frozen: constrained from radio)
		1 keV flux density (nJy)	$1.00^{+1.80}_{-0.13}$
		KT (keV)	$1.12^{+0.39}_{-0.28}$
		Unabsorbed flux (erg s^{-1} cm^{-2})	$\left(1.82^{+0.72}_{-1.10}\right) \times 10^{-14}$
		$\chi^2_{\rm red}$	0.55
NW1 lobe	Power law	Γ	1.95 (frozen)
		1 keV flux density (nJy)	$1.04^{+1.12}_{-1.12}$
		$\chi^2_{\rm red}$	1.47
		Γ	1.788 (frozen)
		1 keV flux density (nJy)	$0.99^{+0.91}_{-0.91}$
		$\chi^2_{\rm red}$	1.53

Note. The observed part (0.3–7.0 keV) of the spectrum has been integrated to find the flux of the apec model.

with those being IC X-rays. However, when we fitted with a pure apec model, we got a good fit also to this model (see Table 6) with a temperature of $1.15^{+0.34}_{-0.22}$ keV, which is marginally higher than the thermal ambient medium ($0.81^{+0.08}_{-0.08}$ keV) constrained by the double background subtraction method. The value of $\chi^2_{\rm red}$ for the apec model fit is 0.51. So, from the fit, it is difficult to distinguish which model to accept as both the power-law and apec models are a good fit individually. We tried to fit a composite model consisting of a power law and an apec model. The best-fitting parameters of this composite model are tabulated in Table 6. In the fit of the composite model, we obtained a best-fitting value of the temperature of $1.00^{+1.80}_{-0.13}$ keV, which is consistent (within the error) with the ambient medium temperature of $0.81^{+1.80}_{-0.13}$ keV. While fitting the spectra with this composite model, we freeze the photon index to 1.788, which is predicted independently from the injection spectral index constrained from the radio spectrum. If we freeze the photon index to 1.95 (obtained from the fit of a single power law to the X-ray spectrum), the best-fitting temperature of the composite models comes out to be similar. So, at least we can conclude that there has been no significant heating of the thermal medium around the lobes due to lobe expansion. All this analysis is for the SE1 lobe of J1158+2621. The number of counts was not enough to constrain the X-ray spectrum of the NW1 lobe. So we freeze the photon index (i) to 1.95 as obtained from the single power-law fit to the X-ray spectrum and (ii) to 1.788 as predicted from the radio spectrum (Konar et al. 2013) and fit with the observed spectrum twice. We obtain a reasonable fit to a single power law in both the cases (see Table 6). The fit parameters for the fits with photon indices of 1.95 and 1.788 are quite similar, with similar $\chi^2_{\rm red}$ values (see Table 6).

We are fully aware that in J1158 the background subtraction based on an off-lobe region is improper if the lobes significantly affect the atmosphere, and this is common in cluster radio galaxies. In that case our model fitting would be incorrect and an incorrect model would change the IC flux as well as the spectral index. However, we could not do any sophisticated analysis with this data. So any interpretation with these results should be taken with caution.

4.3 J1548−3216

For this source also a detailed spectral ageing analysis has been done by Machalski, Jamrozy & Konar (2010). For the lobes, the injection spectral indices constrained by them from the radio spectra are 0.583 and 0.540 for the SE1 lobe and NW1 lobe, respectively. Konar and Hardcastle (2013) fitted the total spectrum of both outer lobes and obtained an injection index of 0.567. So, if the radio spectra are well constrained, we may expect a photon index of around 1.567 for the IC X-ray from the lobes. The two lobes of this source have mixed with each other near the core and the entire source looks like a single lobe. Since the radio injection indices are not so different for the two lobes, we can treat the entire source to be the same source while constraining the spectra of lobe-related X-ray. We could not constrain the X-ray spectrum of the core, which is very weak.

Table 7. Fit statistics of the background spectra of the environment of J1548−3216. Only data from the MOS1 and MOS2 cameras have been used. Because of the higher systematics, data from pn camera could not yield any reasonable fit.

Model component (1)	Model parameter (2)	Best-fitting value (3)	(4)
Background spectrum-1	kT (keV)	$0.29^{+0.01}_{-0.01}$	
	Abundance ($Z_\odot$)	1 (frozen)	
	Redshift	0 (frozen)	
	Norm (cgs)	$\left(2.13^{+0.18}_{-0.18}\right) \times 10^{-4}$	
Background spectrum-2	kT (keV)	$0.071^{+0.067}_{-0.026}$	
	Abundance ($Z_\odot$)	1 (frozen)	
	Redshift	0 (frozen)	
	Norm (cgs)	$\left(2.92^{+110}_{-2.77}\right) \times 10^{-3}$	
Background spectrum-3	$N_{\rm H}$ ($\rm cm^{-2}$)	0.077×10^{22} (frozen)	
	Photon index[a]	1.41 (frozen)	
	Norm ($N_{\rm 1keVph}$ $\rm s^{-1}$ $\rm cm^{-1}$)	$\left(1.03^{+0.01}_{-0.01}\right) \times 10^{-4}$	
Spect 1,2, and 3 together			$\chi_{\rm red} = 1.05$
Thermal ambient medium	$N_{\rm H}$ ($\rm cm^{-2}$)	0.077×10^{22} (frozen)	
	kT (keV)	$0.20^{+0.38}_{-0.10}$	
	Abundance ($Z_\odot$)	0.3 (frozen)	
	Redshift	0.1082 (frozen)	
	Norm (cgs)[b]	$\left(1.30^{+2.64}_{-1.17}\right) \times 10^{-4}$	

[a]When we fitted three background spectra, we froze the photon index of the CXB at 1.41. However, during fitting of the spectrum of the thermal ambient medium a CXB photon index of 1.41 yields a bad fit to the normalization of the spectrum of the thermal ambient medium (though it yields a similar best-fitting temperature). So, we thawed this parameter during the fitting of the spectra of the background and thermal ambient medium together. The best-fitting value of this parameter we obtained is $1.12^{+0.18}_{-0.18}$. This yields relatively better normalization to the spectrum of the thermal ambient medium.
[b]This will be kept free when the lobe-related X-ray is fitted.

4.3.1 *Environment*

We have been able to employ the double background subtraction method for constraining the spectrum of the thermal medium around the host galaxy of J1548−4722. We were able to use MOS1 and MOS2 data for the double background subtraction method for constraining the thermal X-ray spectrum of the ambient medium. The best-fitting values are given in Table 7. The best-fitting temperature of the ambient medium is $0.20^{+0.38}_{-0.10}$ keV, which is again consistent with a very poor group scale environment as in the case of J1158+2621. Spectral extraction regions for the environment have been shown in Fig. 3.

4.3.2 *Lobes*

We have constrained the lobe spectra for both the lobes together. For the details of the lobe extraction and the background subtraction regions see Sectin 4.4. The best-fitting values of the parameters of the models fitted are tabulated in Table 8. Since we set a background subtraction region far away from the core position, the spectra from the lobe region in principle may contain two components: (i) IC X-rays from the radio lobes and (ii) thermal X-rays from the ambient medium. Initially we fitted a single power law; then we fitted a composite model consisting of a power law and an apec model. The best-fitting photon index and the normalization of the power law in both the cases are similar within the error. In the composite model, we freeze the temperature, as otherwise it was difficult to get any reasonable best-fitting values. Freezing the temperature of the apec model means that we are essentially assuming that there is no significant detectable shock-heated emission associated with the lobe expansion. This is largely true for most of the radio lobes (Croston et al. 2004, 2005; Konar et al. 2009) of large radio galaxies.

4.4 Details of spectral extraction regions

For constraining lobe spectra of J0116-4722, the source extraction and background subtraction regions for N1 and S1 lobes are shown in the top panel os Fig. 4. The sizes of the lobe extraction regions for this source are given in the caption of Fig. 4. Spectral extraction region of core spectra of J1158+2621 is shown in Fig. 5. For constraining lobe spectra, the lobe extraction and background subtraction regions of J1158+2621 are ellipses of same sizes as shown in Fig. 5. The chip gap regions in the field of J1158+2621 are rectangular as shown in Fig. 5. Chip gap regions have to be excluded from the analysis. The shapes and sizes of lobe extraction regions of J1548-3216 are given in the caption of Fig. 6.

5 CONSTRAINING MAGNETIC FIELDS IN THE LOBES

All our episodic radio galaxies are FR II radio galaxies, so the radio lobes contain the downstream plasma (fluid) of the jet termination

Table 8. Fit statistics of the spectra of the lobes of J1548−3216 ($N_{\rm H} = 0.077 \times 10^{22}$, $z = 0.1082$).

Source Component (1)	Model (2)	Parameter (3)	Best-fitting values (4)
All lobes together	Power law	Γ	$2.11^{+0.40}_{-0.42}$
	(preferred model)	1 keV flux density (nJy)	$28.27^{+4.74}_{-4.97}$
		$\chi^2_{\rm red}$	1.59
	apec + power law	Γ	$1.82^{+0.64}_{-0.56}$
		1 keV flux density (nJy)	$25.10^{+7.18}_{-7.62}$
		kT (keV)	0.20 (frozen)
		Unabsorbed flux (erg s^{-1} cm^{-2})	$\left(2.30^{+3.63}_{-2.30}\right) \times 10^{-14}$
		$\chi^2_{\rm red}$	1.60

Note. The observed part (0.3–7.0 keV) of the spectrum has been integrated to find the flux of the apec model.

shocks (see Konar & Hardcastle, 2013). These particles (i.e. electrons and positrons) are radiating in radio wavelengths via the synchrotron process and in X-ray wavelengths via Inverse-Compton scattering against Cosmic Microwave Background photons (IC-CMB process). The synchrotron emissivity depends on the radiating particle density ($n_{\rm e}$) and the strength of the magnetic field (B) and both are unknown for a given lobe. IC-CMB emissivity of the same lobe depends on $n_{\rm e}$ (which is unknown) and CMB energy density ($U_{\rm CMB}$). In this case, $U_{\rm CMB}$ for any given lobe is known if we know the redshift of the source. Therefore, from IC-CMB, if detected in a lobe, $n_{\rm e}$ can easily be constrained. Once we put the value of $n_{\rm e}$ in the synchrotron emissivity formula, we can essentially constrain the magnetic field of the lobe considered (Croston et al. 2004; Hardcastle et al. 2004; Croston et al. 2005; Konar et al. 2009). We have estimated the equipartition magnetic field of the outer lobes of our small sample of DDRGs and constrained the magnetic field of those lobes using the SYNCH code of Hardcastle, Birkinshaw & Worrall (1998). We have used a power-law synchrotron spectral model with a high-frequency break corresponding to the Jaffe–Perola model (Jaffe & Perola 1973; Konar et al. 2006). Table 9 lists the magnetic fields that we constrained for the outer lobes along with their equipartition magnetic fields.

For J0116−4722, a single power law is the only acceptable model for fitting the lobe-related X-ray spectra. The lobes of this source are close to equipartition condition.

For the SE1 lobe of J1158+2621, we found that both a single power law and an apec model were good fits individually. We also fitted a composite model consisting of a power law and an apec model. This is a reasonable fit, though the fit parameters have larger errors. If we fit a single power law and the composite model, the best-fitting values of the 1 keV flux densities for the power-law components in two cases are 3.46 and 1.00 nJy, respectively (see Table 6). Hence we estimated the true value of B for both values of 1 keV flux densities (see Table 9). In both cases we found that the true value of B is within a factor of 2 of the equipartition value.

For the source J1548−3216 we have constrained the magnetic fields from the radio spectra with $\alpha_{\rm inj} = 0.567$ (constrained from radio spectra by Konar & Hardcastle 2013) and $\alpha_{\rm inj} = 0.82$ (as obtained from the photon index of the power law fitted to the lobe-related X-ray spectrum). An injection index of 0.567 (which is flatter than the 0.62 predicted by Kirk et al. 2000 from the particle acceleration model) is not consistent with the shock acceleration model of Kirk et al. (2000). Since the particle acceleration model of Kirk et al. (2000) is consistent with the observations (see Konar & Hardcastle 2013), we prefer to accept $0.82^{+0.64}_{-0.56}$ as a good measure of the injection spectral index for this source. If the true injection spectral index is around 0.82, then the lobes of J1548−3216 are very close to equipartition condition.

We conclude that the outer lobes of the DDRGs have magnetic fields very close to the equipartition values. Even though the replenishment of energetic particles in the outer lobes has stopped, the lobes are still as close to the equipartition condition as in currently active objects. The spectral ages of the outer double of these DDRGs are 66–236 (limits), 113, and 74 Myr for J0116−4722, J1158+2621, and J1548−3216, respectively, using an equipartition magnetic field assumption (Machalski, Jamrozy & Konar 2010; Konar et al. 2013). The spectral ages of a sample of smaller sources studied by Leahy, Muxlow & Stephens (1989) have been reestimated by Jamrozy et al. (2008) using the current cosmological parameters. They found that the median spectral ages of the smaller (100 kpc scale) radio galaxies are 8 Myr. So, the spectral ages of outer doubles of our sample of DDRGs are likely to be significantly older than the few 100-kpc-scale radio galaxies studied by Croston et al. (2005). In spite of that, we observe that the outer doubles of our DDRGs are very close to energy equipartition between magnetic field and radiating particles. This suggests that the magnetized relativistic plasma remains in energy equipartition not only when it is freshly pumped into the lobes but also when it gets older, after the energy injection by the jets stops. This is direct evidence that relativistic radio-emitting plasma remains close to energy equipartition between the magnetic field and the particles on time-scales between a few Myr to ∼100 Myr.

6 MODE OF ACCRETION

High-excitation radio galaxies (HERGs) and low-excitation radio galaxies are thought to operate in two different modes of accretion, respectively radiatively efficient and radiatively inefficient (e.g. Hardcastle, Evans & Croston 2007). The nuclei of HERGs show strong [O III] lines in the optical spectra and in mid-infrared (mid-IR: ∼20 μm) the AGNs of HERGs are often strong sources due to their torus emission. In X-ray wavelengths in the 0.3–10 keV rest-frame frequency band of *XMM*, the spectrum of HERGS can

Table 9. A comparison of equipartition magnetic field and true magnetic field of the outer lobes of the DDRGs is shown here. The column designations are as follows. Column 1: the name of the source; column 2: the source component; column 3: the injection spectral index as constrained from the radio spectrum (Konar & Hardcastle 2013), which has been used in predicting the IC-CMB X-ray flux; column 4: 1-kev observed flux density as obtained by constraining the X-ray spectra of the outer lobes of the DDRGs (the true B in lobes has been adjusted so that the predicted IC-CMB flux density at 1 keV matches with this observed value); column 5: equipartition magnetic field estimated with the SYNCH code; column 6: the true magnetic field of the outer lobes of the DDRGs constrained by IC-CMB modelling (using the SYNCH code); column 7: the ratio of the equipartition magnetic field to the true magnetic field.

Source	Components	1-kev X-ray flux density (nJy)	$\alpha_{\rm inj}$ (radio)	$B_{\rm eq}$ (nT)	$B_{\rm IC}$ (nT)	$\frac{B_{\rm eq}}{B_{\rm IC}}$	$\alpha_{\rm inj}$ (IC X-ray fitting)	$B_{\rm eq}$ (nT)	$B_{\rm IC}$ (nT)	$\frac{B_{\rm eq}}{B_{\rm IC}}$
(1)	(2)	(3)	(4)	(5)	(6)	(7)	(8)	(9)	(10)	(11)
J0116−7422	N1 lobe	19.36	0.618	0.212	0.121	1.75	0.77[f]	0.294	0.165	1.78
	S1 lobe	18.17	0.618	0.223	0.150	1.49	1.00[e]	0.539	0.311	1.73
J1158+2621	NW1 lobe	1.04	0.788	0.531	0.508	1.04	0.95[d]	0.770	0.630	1.22
	SE1 lobe	3.46[a]	0.788	0.552	0.288	1.92	0.95[d]	0.800	0.370	2.16
	SE1 lobe	1.00[b]	0.788	0.552	0.560	0.99				
J1548−3216	Both lobes	25.10	0.567	0.226	0.068	3.32†	0.82[c]	0.226	0.133	1.70

[a]This is the 1 kev flux density constrained by fitting a single power-law model to the lobe-related X-ray spectra.
[b]This is the 1 kev flux density of the power-law component, constrained by fitting a composite model consisting of a power law and an apec model.
[c]This is the injection spectral index estimated from the photon index constrained by fitting a composite model (a power law + an apec model) to the lobe-related X-ray spectra of both the lobes together.
[d]This is the injection spectral index estimated from the photon index constrained by fitting a power-law model to the lobe-related X-ray (Table 6). The injection spectral index from the composite model (power law + apec model) fitting would have been good; however, we had frozen the injection spectral index for the composite model and not constrained it.
[e]We have taken the injection spectral index from power-law fitting (Table 3), not from the composite model, as unabsorbed flux is very poorly constrained in the composite model.
[f]We have taken the injection spectral index from power-law fitting (Table 3), not from the composite model, as temperature is very poorly constrained in the composite model.
†There seems to be a departure from equipartition if we use the injection spectral index of 0.567 to predict the 1 kev IC-CMB flux density.

be fitted with a double power law: an unobscured soft power law and an obscured hard power law. The soft power law is jet-related X-ray (Hardcastle et al. 2009) appearing in the relatively softer regime of the *XMM* band and could be a mixture of synchrotron, synchrotron self Compton, and IC-CMB. The soft power law is slightly absorbed only by the Galactic neutral hydrogen, and not absorbed by the material associated with the AGNs. However, the hard power law is heavily absorbed by the torus material of the AGNs (see the spectra of 3C 457 published by Konar et al. 2009 and references therein). The HERGs have a standard accretion disc (Shakura & Sunyaev 1973) and the X-rays in the hard power law is the inverse Comptonized UV radiation from the accretion disc. These hard X-rays come from close to the nuclear regions and intercept the so-called molecular torus depending upon the orientation of the AGNs of the HERGs with the LoS. By contrast, the LERGs have neither torus nor the standard accretion disc. So they are not luminous at mid-IR frequencies, nor do they show [O III] line emission. Moreover, they show only the soft power-law component in the X-ray band of *XMM* and show no hard power-law-related to the accretion disc. Since jets are formed, there must be accretion of matter, which leads to the conclusion that LERGs must accrete matter in a radiatively inefficient mode.

When we look at our small sample of DDRGs carefully, we find that all the DDRGs in our sample are most likely LERGs (see Figs 1–3). With the possible exception of J0116−4722 (see the discussion of its core spectrum above), these DDRGs do not show any absorbed hard power-law component in their X-ray spectra in the*XMM* band, nor are they detected in *WISE* band 4 (22 μm). Two of them do not show any [O III] lines in the optical spectra, and although Danziger & Goss (1983) mentioned the detection of [O III] lines in J0116−4722, they did not publish any spectrum of J0116−4722, nor did they explicitly give quantitative parameters of the strength of the [O III] lines, such as the equivalent width: Further observations would be needed to classify J0116−4722's emission-line spectrum. However, the absence of a hard power law in the *XMM* band and the non-detection of the source in *WISE* band 4 suggest that J0116−4722 is an LERG. The fact that some DDRGs can be LERGs, demonstrated by this work,[1] is important in understanding the nature of the episodic activity and we discuss this point further in the next section.

7 THE CAUSE OF EPISODIC BEHAVIOUR

Radio galaxies (both FR I and FR II) are known to be episodic (FR I: Burns, Feigelson & Schreier 1983; FR II: Schoenmakers et al. 2000a; 2000b; Saikia, Konar & Kulkarni 2006). When a radio galaxy shows episodic behaviour, it is called an ERG; when an ERG shows two episodes of jet activity visible in the same pair of radio lobes, it is called a DDRG.

It is well known (e.g. Laing & Peacock 1980) that FR II radio galaxies can in principle be LERGs or HERGs. The radio galaxies at the centre of cool-core clusters tend to be LERGs (Hardcastle et al. 2007), are thought to be fuelled by accretion from the hot phase, and would naturally be expected to be episodic in nature due to feedback between the SMBHs and the hot gas in the ambient media, with episodic activity taking place on a time-scale of the order of the cooling time corresponding to the central matter density of the cluster (hereafter, we refer to this as the feedback model). It is hard to see how a comparable model can be constructed for high-accretion-rate objects (HERGs) where accretion from the hot medium is

[1]Other episodic radio galaxies have been shown to be LERGs, e.g. 4C 32.26 (Jetha et al. 2008), but these were not double–double sources.

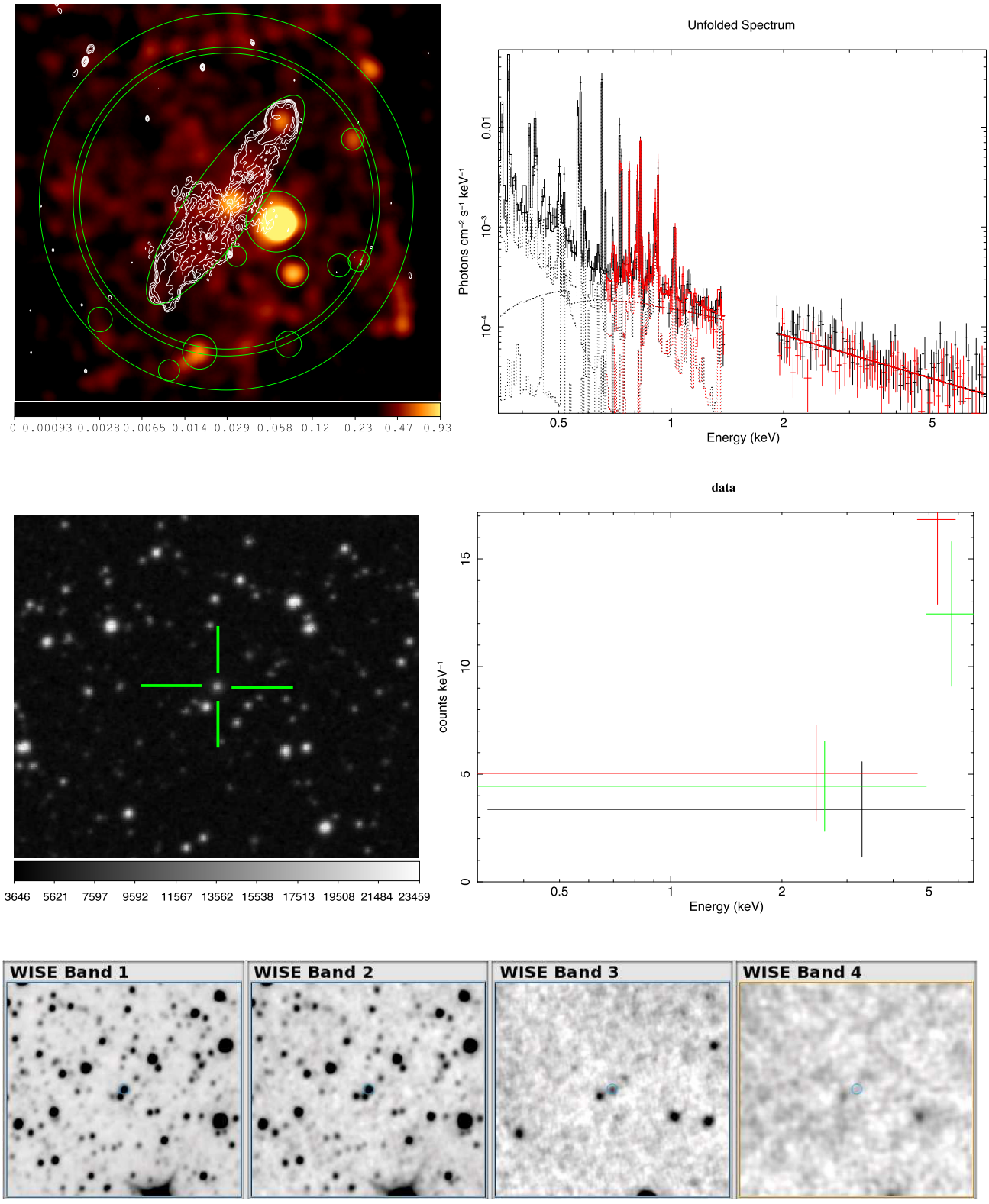

Figure 3. X-ray, radio, optical and mid-IR properties of J1548−3216. Upper left-hand panel: an overlay of an X-ray image and GMRT 610 MHz radio image with the regions selected for the spectral extraction for the environment by the double background method. The first radio contour is 0.5 mJy beam^{-1} and other contours increase by factors of 2. Upper right-hand panel: the fit to the total spectrum containing all the components, e.g. three background spectra and the thermal ambient medium spectrum. The data between 1.4 and1.9 kev have been flagged as there is a prominent instrumental aluminium line. Middle left-hand panel: DSS2R image of the field. The host galaxy is indicated by the cross. Middle right-hand panel: the X-ray spectra of the core. Lower panel: *WISE* images in 4 bands. The source is not detected in *WISE* band 4.

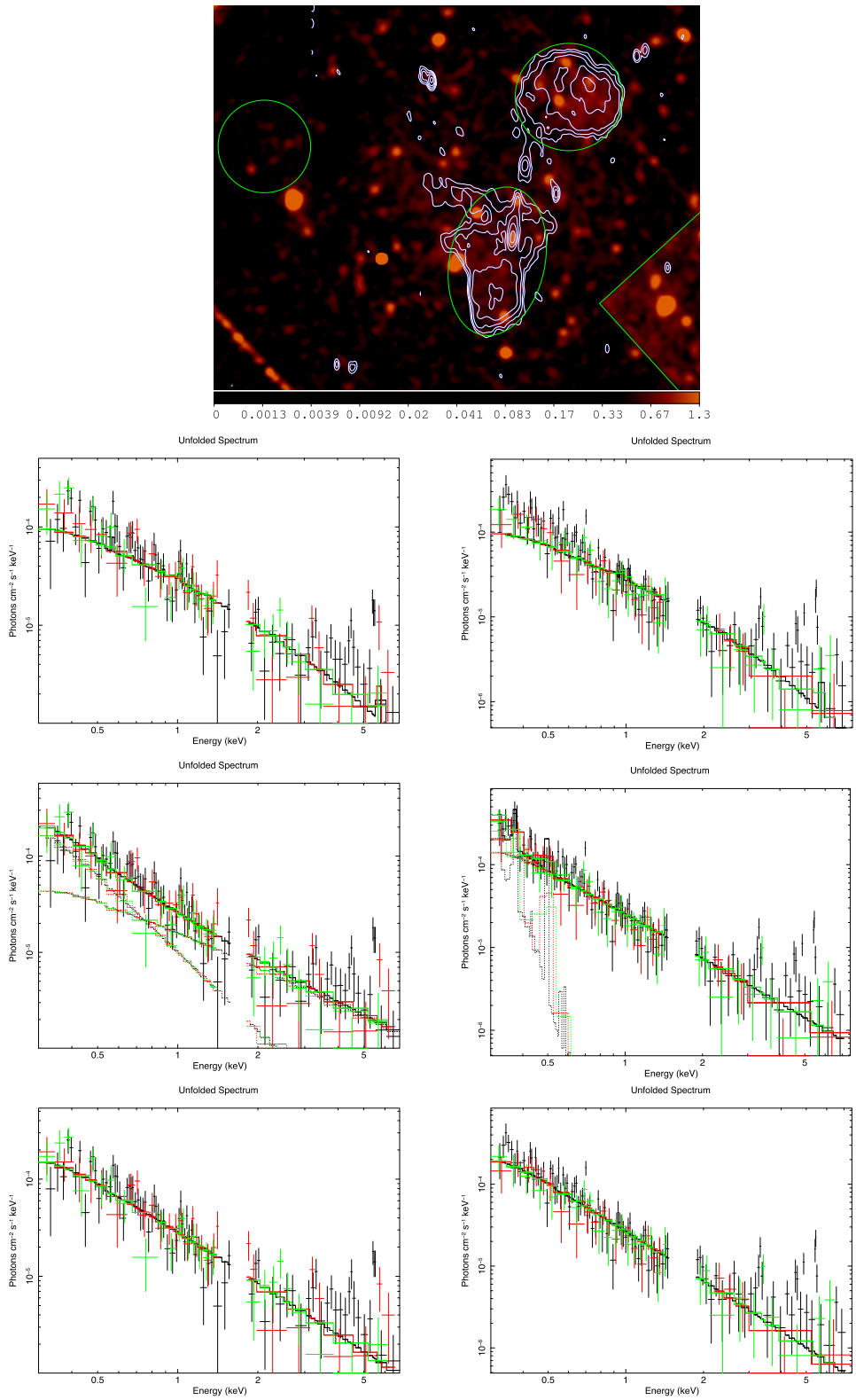

Figure 4. The lobes of J0116−4722. Top panel: an X-ray image (colour) and a radio 334 MHz GMRT image (contour) have been overlaid. The outermost radio contour corresponds to 5 mJy beam^{-1} and higher contours increase by factors of 2. Lobe extraction regions of J0116−4722 have been shown by a circle (for the N1 lobe) and an ellipse (for the S1 lobe). The diameter of the circle around the N1 lobe is 240 arcsec. The elliptical region around the S1 lobe has a major axis of 360 arcsec and a minor axis of 240 arcsec. The background region is shown by a circle far from the source. The triangular region to the west of the S1 lobe is the data from a bad chip. Lower panels: lobe spectra of J0116−4722, fitted with various models. The lobe spectra fitted with an apec model, a composite model (an apec plus a power law), and a single power law are shown from top to bottom, respectively. Lower left-hand panels: Fits to the N1 lobe. Lower right-hand panels: fits to the S1 lobe.

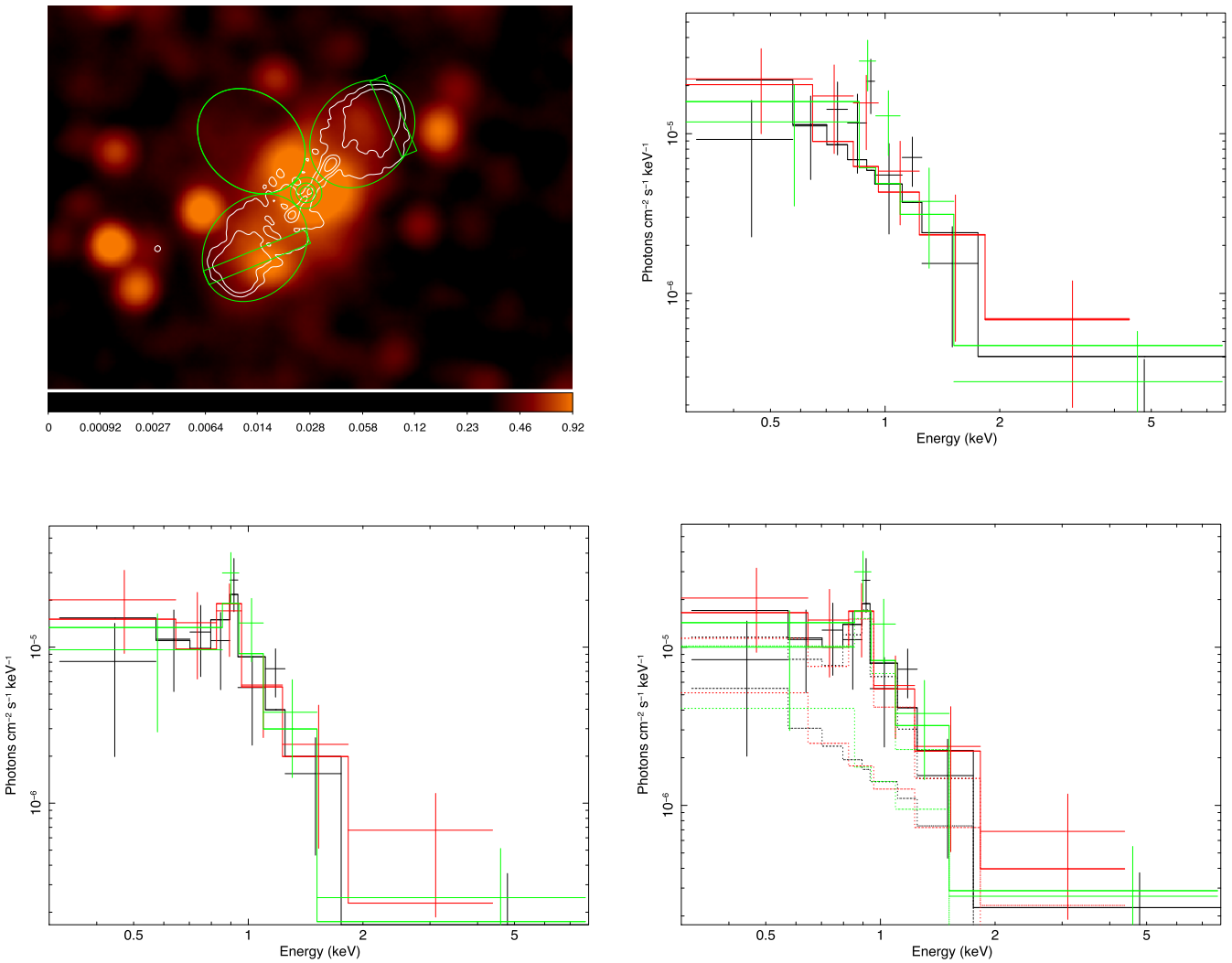

Figure 5. The lobes of DDRG J1158+2621. Upper left-hand panel: lobe spectral extraction and background regions. The ellipses around the NW1 lobe, the SE1 lobe, and the elliptical background region have the same size with a major axis of 124.3 arcsec and a minor axis of 99 arcsec. Upper right-hand panel: the X-ray spectrum of the SE1 lobe has been fitted with a power law. Lower left-hand panel: the X-ray spectrum of the SE1 lobe fitted with an apec model. Lower right-hand panel: a composite model of a power law and an apec model fit to the X-ray spectra.

thought to be insufficient to produce the observed radiative and kinetic output, since in this case the source of fuel is basically unaffected by the activity of the radio galaxy; if episodic activity is purely due to feedback, then ERGs must in general be LERGs (which, however, is known not to be the case: the DDRG 3C 219 is a broad-line radio galaxy and hence a HERG).

Other explanations of DDRG activity are possible. There have been suggestions that multiple encounters during a galactic merger (hereafter, galactic-merger model: Schoenmakers et al. 2000a) could be the cause of the multiple episodes of FR II ERGs. However, there is as yet no observational evidence that DDRGs differ in terms of their merger state from other radio galaxy hosts. Saripalli & Mack (2007) reported that there is no indication of molecular gas mass larger than a few 10^8–10^9 $M_\odot$ for a sample of nine DDRGs. Their study suggests that the DDRGs are as deficient in molecular gas as the normal FR II radio galaxies. So there seems to be no accumulation of molecular gas in DDRGs in the recent past, which is inconsistent with the galactic-merger explanation of ERG behaviour. Saripalli & Mack (2007) suggested instead that the cessation of jet activity and the subsequent restarting of jets in DDRGs might be due to instabilities in the fuelling processes rather than the depletion of, and subsequent acquisition of, fuel. One of our sample sources, namely J1158+2621 (4C 26.35), is part of their sample too, and in general their sources are similar to ours, so we expect that galactic mergers are not the cause of episodic behaviour in our sources.

Liu, Wu & Cao (2003) proposed that the disruption of the inner part of the accretion disc due to coalescence of binary black holes of unequal mass (e.g. a mass ratio of 10:1) can cause the cessation of jet activity (hereafter the BBH model). Then the truncated disc will extend to the innermost stable circular orbit (ISCO) on a viscous time-scale and the jet activity would start again. For the BBH model to work, the ERGs have to be HERGs, or in other words there has to be standard accretion discs in the central engines; this model does not work for the hot accretion flow where there is no standard accretion disc (Liu et al. 2003). Though the galactic merger can

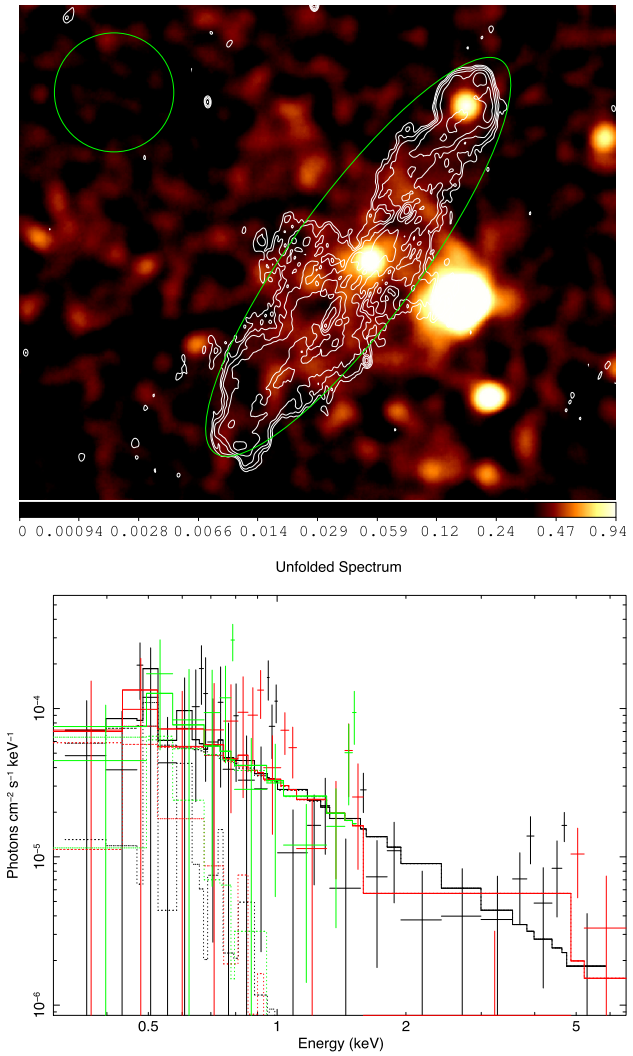

Figure 6. Top panel: the lobe spectrum extraction region and the background subtraction region. The ellipse around the entire source has a major axis of 422 arcsec and a minor axis of 138.5 arcsec. Bottom panel: the spectrum of the lobe-related X-rays of J1548−3216. Both the lobes have been considered together. The observed spectra have been fitted with a power law and an apec model.

be traced via detection and measurements of a molecular gas disc and/or dust lane around the BH, the BH merger that has caused the jet interruption in DDRGs cannot be traced, as the merger took place before the second episode started, and so in this sense it is harder to constrain the BBH model; but our sample DDRGs are all LERGs, lacking standard accretion discs, and therefore we can rule out the simplest versions of the BBH model as proposed by Liu et al. in our attempt to explain the cause of episodic behaviour in our sample of DDRGs. The only possibilities remaining are the feedback model and the possibility that the accretion mode of the sources has actually changed over time: Change of mode of accretion can also be connected with instabilities in the fuel supply, as the mode of accretion has a dependence on the temperature of the fuel and the mass accretion rate.

For our sample of DDRGs, the duration of the quiescent phase is 10^5–10^7 yr (Konar et al. 2013), and the upper end of this range is certainly comparable to the central cooling times found in the centres of RG-hosting groups (Hardcastle & Worrall 2001). It would be desirable to test the feedback model by comparing the quiescent times directly to the central cooling time of the hot phase in these objects, but our existing *XMM* data are not good enough to carry out radial profile fitting to the ambient medium, nor do they have the resolution to give us a good measure of the central cooling time. This test must await future observations.

8 SUMMARY

We have reported on the X-ray observations of a sample of three DDRGs. We observed that all our sample DDRGs are LERGs, which allows us to rule out the Liu et al. (2003) model as the cause of episodic behaviour for our sample of DDRGs. The outer lobes of our sample of DDRGs show small departures from equipartition field strengths consistent with what is observed in active radio galaxies, though the outer lobes are basically relic lobes. This is the first time that it has been possible to show that even the relic lobes of DDRGs are close to the equipartition condition. Future X-ray observations with larger samples, and studies of the mode of accretion in a larger sample of DDRGs, will verify the universality of these results.

ACKNOWLEDGEMENTS

CK thanks the School of Physics, Astronomy and Mathematics at the University of Hertfordshire, where a major part of this research was done, for their hospitality. AH is thankful to the University Grants Commission (India) for the one-time start-up and monthly salary grants, under the Faculty Recharge Programme. This research has made use of the NASA/IPAC extragalactic data base, which is operated by the Jet Propulsion Laboratory, Caltech, under contract with the National Aeronautics and Space Administration. We thank the GNU/Linux group for their contribution. CK acknowledges Ronald Taam for discussion on various theoretical issues. MJH and JHC acknowledge support from the UK Science and Technology Facilities Council [ST/M001008/1 and ST/R00109X/1.]. MJ was supported in part by the National Science Centre, Poland, grant 2018/29/B/ST9/01793.

REFERENCES

Bagchi J. et al., 2014, ApJ, 788, 174
Burns J. O., Feigelson E. D., Schreier E. J., 1983, ApJ, 273, 128
Croston J. H., Birkinshaw M., Hardcastle M. J., Worrall D. M., 2004, MNRAS, 353, 879
Croston J. H., Hardcastle M. J., Birkinshaw M., Worrall D. M., Laing R. A., 2008, MNRAS, 386, 1709
Croston J. H., Hardcastle M. J., Harris D. E., Belsole E., Birkinshaw M., Worrall D. M., 2005, ApJ, 626, 733
Danziger I. J., Goss W. M., 1983, MNRAS, 202, 703
Dickey J. M., Lockman F. J., 1990, ARA&A, 28, 215
Fabian A. C., 2012, ARA&A, 50, 455
Fanaroff B. L., Riley J. M., 1974, MNRAS, 167, 31
Hardcastle M. J., Evans D. A., Croston J. H., 2009, MNRAS, 396, 1929
Hardcastle M. J., , Worrall D. M., , 2001, ASPC, 250:234
Hardcastle M. J., Birkinshaw M., Worrall D. M., 1998, MNRAS, 294, 615
Hardcastle M. J., Evans D. A., Croston J. H., 2007, 376, 1849
Hardcastle M. J., Harris D. E., Worrall D. M., Birkinshaw M., 2004, ApJ, 612, 729
Hota A. et al., 2011, MNRAS, 417, L36
Ineson J., Croston J. H., Hardcastle M. J., Mingo B., 2017, MNRAS, 467, 1586
Jaffe W. J., Perola G. C., 1973, A&A, 26, 423

Jamrozy M., Konar C., Machalski J., Saikia D. J., 2008, MNRAS, 385, 1286
Jamrozy M., Saikia D. J., Konar C., 2009, MNRAS, 399L, 141
Jetha N. N., Hardcastle M. J., Ponman T. J., Sakelliou I., 2008, MNRAS, 391, 1052
Kirk J. G., Guthmann A. W., Gallant Y. A., Achterberg A., 2000, ApJ, 542, 235
Konar C., Hardcastle M. J., 2013, MNRAS, 436, 1595
Konar C., Hardcastle M. J., Croston J. H., Saikia D. J., 2009, MNRAS, 400, 480
Konar C., Hardcastle M. J., Jamrozy M., Croston J. H., 2013, MNRAS, 430, 2137
Konar C., Hardcastle M. J., Jamrozy M., Croston J. H., Nandi S., 2012, MNRAS, 424, 1061
Konar C., Saikia D. J., Jamrozy M., Machalski J., 2006, MNRAS, 372, 693
Kuźmicz A., Jamrozy M., Kozieł-Wierzbowska D., Weżgowiec M., 2017, MNRAS, 471, 3806
Laing R. A., Peacock J. A., 1980, MNRAS, 190, 903
Leahy J. P., Muxlow T. W. B., Stephens P. W., 1989, MNRAS, 239, 401
Liu F. K., Wu X.-B., Cao S. L., 2003, MNRAS, 340, 411
Machalski J., Jamrozy M., Konar C., 2010, A&A, 510, A84
McNamara B. R., Nulsen P. E. J., 2007, ARA&A, 45, 117
Mulcahy D. D. et al., 2016, A&A, 595L, 8
Nandi S. et al., 2014, ApJ, 789, 16
Osmond J. P. F., Ponman T. J., 2004, MNRAS, 350, 1511
Saikia D. J., Konar C., Kulkarni V. K., 2006, MNRAS, 366, 1391
Saripalli L., Mack K.-H., 2007, MNRAS, 376, 1385
Schoenmakers A. P., de Bruyn A. G., Röttgering H. J. A., van der Laan H., 2000b, MNRAS, 315, 395
Schoenmakers A. P., de Bruyn A. G., Röttgering H. J. A., van der Laan H., Kaiser C. R., 2000a, MNRAS, 315, 371
Shakura N. I., Sunyaev R. A., 1973, A&A, 24, 337

This paper has been typeset from a TEX/LATEX file prepared by the author.